Effect of Nb Content on the Microstructure and Wear Resistance of Fe-12Cr-*x*Nb-4C Coatings Prepared by Plasma-Transferred Arc Welding

Lin Zong [1],*, **Yinglong Zhao** [2], **Shiteng Long** [2] **and Ning Guo** [2],*

1   School of Mechanical and Power Engineering, Shenyang University of Chemical Technology,
    Shenyang 110142, China
2   School of Materials and Energy, Southwest University, Chongqing 400715, China;
    zyl19970611@email.swu.edu.cn (Y.Z.); lst506537971@email.swu.edu.cn (S.L.)
*   Correspondence: zl790429@syuct.edu.cn (L.Z.); guoning_1000@163.com or whc34@swu.edu.cn (N.G.)

Abstract: The Fe-Cr-C coatings with different levels of Nb addition were prepared on carbon steel by a plasma transferred arc (PTA) weld-surfacing process and their microstructure and properties were investigated. As the Nb content increases from 8.96% to 12.55%, the coating gradually changes from a hypereutectic structure (martensite, austenite matrix, primary NbC and eutectic $\gamma+M_7C_3$) to a near eutectic structure ($\gamma+M_7C_3$ and NbC) and finally a hypoeutectic structure (primary γ, $\gamma+M_7C_3$ and NbC). As the Nb content increases, the hardness and wear resistance of the coating first increase and then decrease, which is closely related to the NbC volume fraction first increasing and then the NbC size coarsening. The Fe-Cr-C coating with 11.65% Nb balances the NbC content and size, and has the highest hardness and best wear resistance. As the Nb content increases further, the formation and aggregation of coarse NbC carbides in the coating results in high brittleness of the coating, which may cause the carbide particles to peel off the coating during the wear process, thereby reducing wear resistance.

Keywords: NbC; plasma-transferred arc welding; eutectic; wear resistance

1. Introduction

There are four main types of engineering component failures, namely fracture, corrosion, wear and deformation. Wear accounts for 55% of the total failures, and abrasion accounts for 20% of wear failures [1]. This highlights the importance of studying abrasive wear solutions. Generally, surface modification technology is applied to improve the surface properties of engineering components [2–6]. In surface treatments, usually a suitable powder and a thin surface layer of Fe-based melt are simultaneously and rapidly solidified to produce a compact coating with good metallurgical bonding to overcome surface degradation mechanisms [7].

In order to further improve the wear resistance of Fe-based alloys under severe working conditions, researchers have explored the properties of Fe-Cr-C hardfacing alloys reinforced by the precipitation of MC type carbides [8–13]. Compared to other MC type carbide-forming elements, niobium (Nb) is the strongest carbide-forming element and can combine with carbon in the hardfacing alloy to form granular carbides with high hardness. On the other hand, formation of these carbides reduces the carbon concentration in the matrix of the hardfacing alloy, which is favorable for improving the toughness. Some meaningful and interesting results have been reported in this area [14–19]. For example, Zhang et al. [20] investigated the effect of Nb content on the microstructure of Fe-Cr-C coatings, and discovered that Nb can not only promote the formation of equiaxed grains, but also

make the microstructure become finer. Correa et al. [21] indicated that the excellent properties of hypereutectic Fe-Cr-C-Nb hardfacing alloy deposited by the open arc welding process can be attributed to the presence of fine primary NbC carbide, which randomly disperses in an eutectic matrix γ/M_7C_3. Chung et al. [22] investigated the influence of Nb addition on a hypereutectic alloy system, and they concluded that the final microstructure evolves from hypereutectic to eutectic and hypoeutectic with increasing of Nb contents. Moreover, fine NbC carbides result in superior hardness and wear resistance of the eutectic microstructure.

It is found that increasing Nb content (above 0.71 wt.%) promotes the formation of MC carbides, increasing the wear resistance [23]. Although some progress in the study of the influence of Nb on coatings has occurred, the effect of different niobium contents on the microstructure and wear properties of Fe-Cr-C hardfacing alloys still lacks in-depth research. The focus of the present work is to understand the effects of Nb contents in the coatings on the formation mechanism and distribution characteristics of the microstructure and the wear resistance of coatings with the different Nb contents.

2. Materials and Methods

2.1. Materials and Equipment

Commercial low-carbon steel (ASTM A283 [24]) sheets with a chemical composition of Fe-0.18C-0.35Mn-0.3Si- < 0.04S- < 0.04P (in wt.%) were chosen as the substrate material. Specimens with a size of 100 mm × 80 mm × 12 mm were cut using a wire-electrode cutting machine. Plasma transferred arc (PTA) welding was employed to deposit coatings on the sheet specimens. The composition of the mixed powder used for the PTA treatment was as follows: Fe-66.7%Cr powder, Fe-60%Nb powder, Fe powder (99.0% purity) and graphite (99.5% purity). All the powders were commercially available gas atomized powders and had a spherical shape with a diameter of 75–180 μm. The mixed powders were spread evenly on the sheet specimens. By adjusting the mixed powder ratio (changing the proportion of the Fe-50%Nb content), five kinds of Fe-12Cr-xNb-4C coatings were obtained. The thickness of the coatings was designed to be about 3 mm. The actual chemical composition of the coatings was tested and the results listed in Table 1.

Table 1. Chemical composition (in wt.%) of various hardfacing coatings.

Sample	Cr	Nb	C	Fe
Alloy A	12.34	8.96	3.40	Bal.
Alloy B	12.01	9.86	3.71	Bal.
Alloy C	12.06	10.75	4.01	Bal.
Alloy D	12.11	11.65	4.32	Bal.
Alloy E	12.29	12.55	4.63	Bal.

A plasma powder surface hardening device (DML-V02BD, Shanghai Duomo Industry Co., Ltd., Shanghai, China) was used for the PTA treatment. The PTA processing parameters were as follows: welding current 160 A, voltage 30 V, arc longitudinal movement speed 0.05–0.25 cm/s, arc lateral oscillation frequency 0.35 s^{-1}, arc lateral oscillation width 2.0 cm, arc-workpiece distance 3 mm, flow rate of Ar gas 15 liter/min. Additionally, prior to PTA treatment, the samples were ground using silicon carbide papers from 120# to 800#, and then cleaned with acetone. Meanwhile, in order to increase the adhesion between the mixed powders and the steel, so that the powders are not easily peeled from the steel surface, a small amount of sodium silicate was added to the mixed powders to increase the viscosity of the powder.

2.2. Characterization

A field emission gun scanning electron microscope (FEG-SEM, Nova400, FEI, Hillsboro, OR, USA) equipped with an energy dispersive spectroscopy detector (EDS, Aztec, Oxford Instruments,

High Wycombe, UK) was employed to characterized the microstructure and element distribution of the PTA coatings. The phase components of the coatings were determined by X-ray diffraction experiments (XRD, CuKα, Bruker D8, Bruker AXS GmbH, Karlsruhe, Germany) with the Cu-K radiation at 40 kV and a measuring step of 4°/min. Prior to the characterization, the samples were ground using SiC papers from 800# to 2000#, and then mechanically polished with 3 μm of water-based diamond suspensions on napless clothes.

Hardness tests were performed on a Rockwell hardness tester (HRD-150, Henwall Tech Co., Ltd., Laizhou, China), and five points were tested for each sample. Abrasive wear properties were measured by a rubber wheel abrasion machine (MLS-23, Yihua Tribology Testing Technology Co., Ltd., Jinan, China). The total weight of the quartz sand was 1.5 kg, and the particle size was about 300–500 μm. The testing parameters were as follows: roller diameter 150 mm, rolling speed is 4 r/s, surface pressure of the roller 1.5 MPa, duration time 10 min. Each sample was tested for three times, and the average weight loss value was calculated as the final result.

3. Results

3.1. Phase Composition of the Coatings

Figure 1 shows the XRD spectra of PTA coatings with different Nb contents. It can be seen that although the alloy composition of the five coatings is different, the coating phases are mainly composed of austenite (γ), martensite (M) and alloyed cementite of $(Fe,Cr)_7C_3$ and NbC carbides. However, as the Nb content increases, the relative content of the various phases varies significantly. When the Nb content is relatively low ($\leq$10.75%, see Alloys A, B, and C in Figure 1), the strongest diffraction peaks are located at 44.484°, close to the 110 peak of the M phase and the 211 peak of the $(Fe,Cr)_7C_3$. As the Nb content exceeds 10.75%, the strongest diffraction peak changes to the 111 peak of the NbC located at 34.605° (see Alloys D and E in Figure 1), indicating that the volume fraction of the NbC increases with increasing Nb content. Meanwhile, as the Nb content increases, the intensity of the 200 and 211 diffraction peaks of the M phase decreases, while the intensity of the 200 diffraction peak of the γ phase increases, meaning that the relative contents of M and γ are reduced and increased, respectively.
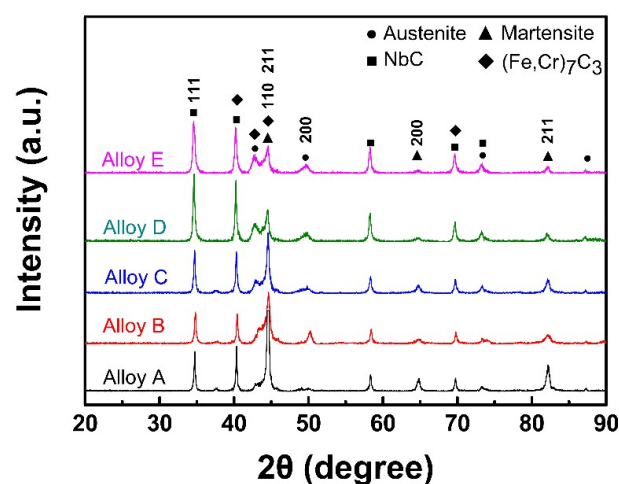

Figure 1. XRD spectra of various coatings with different levels of Nb addition.

3.2. Microstructure of the Coatings

Figure 2 shows optical micrographs observed from the cross-sectional view of Alloy A and Alloy B samples. Crack-free coating, interface and steel substrate can be clearly identified, as shown in Figure 2a,b. The high-magfication images (see Figure 2(a1,b1)) show that the interface is actually a transition-layer/bonding band formed between the coating and the steel substrate, owing to planar

growth at the bottom of the molten pool of the coating. It is the presence of this transition-layer/bonding band that ensures an excellent metallurgical bond between the coating and the substrate. It is considered that the transition-layer/bonding band is favorable to alleviate the stress between the reinforced coating and the steel substate, which is expected to improve the fracture toughness of the coating and the substrate as a whole [25]. In the coating of alloy A, as shown in Figure 2(a2), white bright carbide particles randomly distributed can be clearly seen, which have a flower-like or polygonal shape. Acording to the XRD results (see Figure 1), such paricles are considered to be NbC. With Nb increases from 8.96% to 12.55%, in addition to the white bright carbide particles, a typical eutectic structure is also observed, as shown in Figure 2(b2). This eutectic structure with alternating plates/rods is likely to be γ and alloyed M_7C_3 acording to the XRD results.
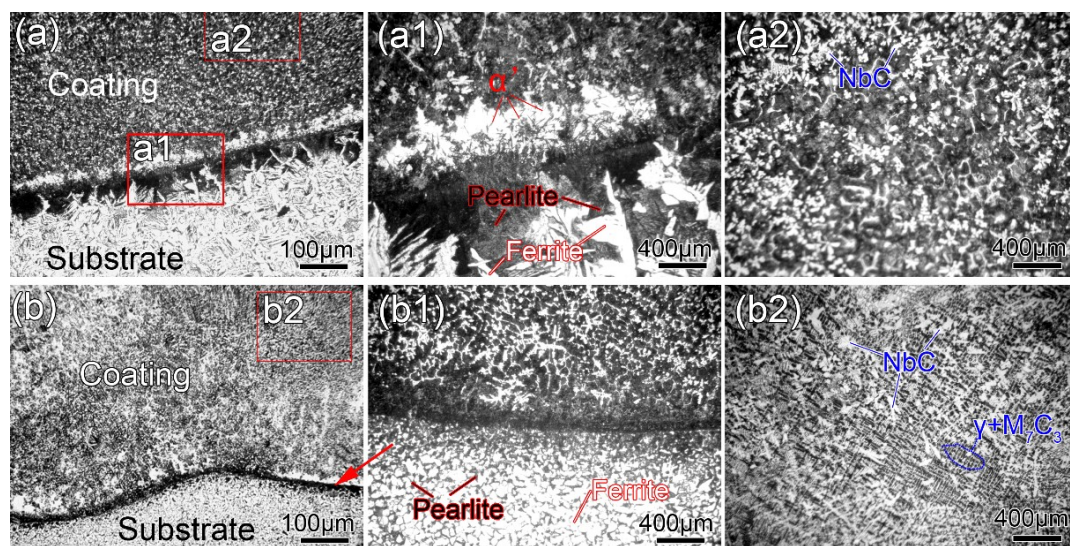

Figure 2. Optical micrographs observed from cross-sectional view of Alloy A (**a**) and Alloy E (**b**). (a1, a2, b1, b2) are the corresponding high-magnification images of the local areas within a and b, respectively.

Figure 3 shows the microstructure of various coatings with different Nb contents. When the Nb content is low (8.96%), as shown in Figure 3a, two types of carbides with different morphology can be easily distinguished: bright white carbides with flower-like or polygonal shapes and cellular carbides. Point analysis was performed using the EDS technique to determine the composition and phase of carbides. The analysis results are collected in Table 2. They show that the white bright carbides are rich in Nb (approximately 76.41%), indicating that these particles are the Nb-rich MC type carbides (see point a1 in Figure 3a and Table 2), while the cellular particles are the $(Fe,Cr)_7C_3$ type carbide (see point a2 in Figure 3a and Table 2) surrounded by the γ phase. Combined with the XRD results, it can be inferred that the coating has a typical hypereutectic structure composed of a primary NbC, eutectic product of $\gamma+(Fe,Cr)_7C_3$. Comparing Figure 3b,c to Figure 3a, it can be seen that even when the Nb content is increased to 10.75%, there is no significant change in the morphology and microstructure of the coating. When the Nb content increases to 12.11%, the microstructure of Alloy D exhibits a near-eutectic characteristic (see Figure 3d), which is mainly composed of the network eutectic constituents and NbC carbides. EDS analysis indicates that the network eutectic structure is composed of eutectic $\gamma+M_7C_3$ (see point d2 in Figure 3d and Table 2). However, as the concentration of Nb increases, the near-eutectic structure is replaced by a hypoeutectic structure (Figure 3e). The EDS analysis and XRD results comprehensively indicate that the microstructure of Alloy E mainly consists of the primary γ, the eutectic structures of $\gamma+M_7C_3$ (see point e2 in Figure 3e and Table 2) and a large amount of coarse dendritic white NbC carbides (see point e1 in Figure 3e and Table 2). Adjacent eutectic structures are interwoven to form the networked structures. During the solidification process, the primary NbC precipitates firstly from the liquid at high-temperature.

With further cooling, the primary NbC carbides grow continuously, meanwhile the eutectic structures of $\gamma + M_7C_3$ precipitate from the remaining liquid phase.
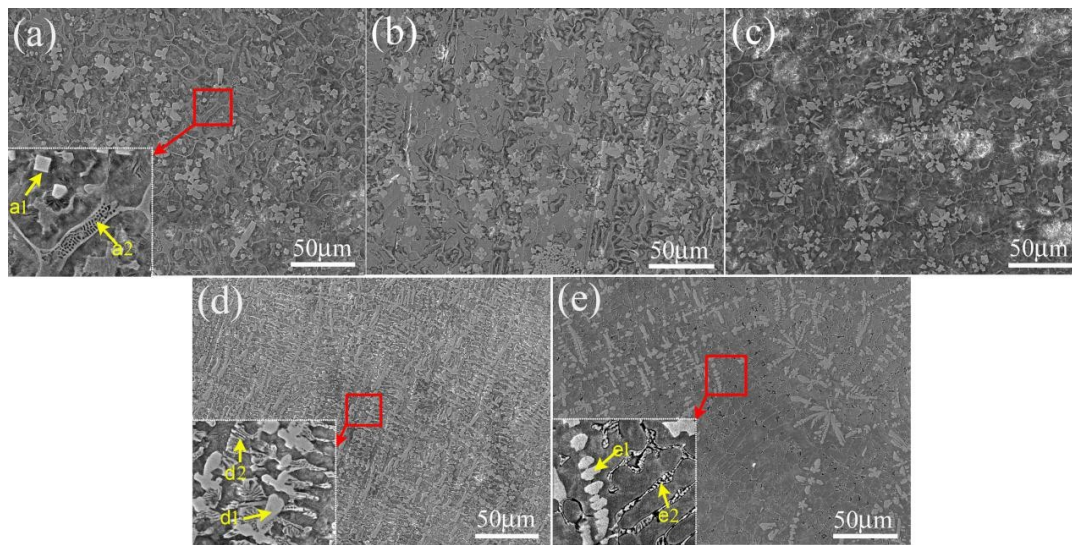

Figure 3. SEM images showing microstructure observed from the surface of various coatings with different Nb additions: (**a**) Alloy A; (**b**) Alloy B; (**c**) Alloy C; (**d**) Alloy D; (**e**) Alloy E.

Table 2. EDS results of the points within Figure 2.

Sample	Position	Content of Components (wt.%)			
		Nb	Fe	Cr	C
Alloy A	a1	76.41	12.65	3.13	7.82
	a2	0.00	76.82	16.94	6.23
Alloy D	d1	79.82	4.12	2.23	13.83
	d2	0.00	65.8	27.5	6.7
Alloy E	e1	81.23	3.44	1.02	14.31
	e2	0.00	57.82	20.67	21.51

Nb is a very strong carbide-forming element, its melting temperature is very high (3500 °C) and has a large negative enthalpy of reaction [26]. Therefore, the formation of niobium carbides is expected to occur in the liquid phase during cooling, which reduces the carbon content in the liquid, thus shifting the structure of the base alloy from a hypereutectic state, through eutectic one, to hypoeutectic one with NbC embedded carbides. Filipovic et al. [27] have demonstrated that by increasing the Nb content in Fe-Cr-C-Nb systems, NbC carbides begin to precipitate first during solidification. The formation of NbC carbides reduces the carbon content of the remaining liquid phase, thereby promoting the formation of the hypoeutectic structure. Additionally, it has been reported that the early precipitation of NbC carbides may promote heterogeneous nucleation and pin austenite grain boundary migration to refine the austenite structure, which is a typical approach used to obtain structure refinement in microalloyed steels [22]. It can also be seen from Figure 3 that the amount of NbC carbides increases with increasing Nb content. This is because as Nb content increases, the nucleation rate of primary carbides increases, resulting in a larger volume fraction of NbC. In some local areas, carbides are closely packed together to form the coarse NbC clusters, which may adversely affect the performance of the coating, e.g., reducing toughness.

Figure 4 presents the higher magnification images of the typical hypereutectic microstructure of Alloy A, near-eutectic of Alloy D, and hypoeutectic of Alloy E. The NbC shape is polygonal and flower-like in the microstructure of Alloy A, NbC has two forms in the microstructure of Alloys D

and E: long strip and cross dendrite. It is considered that the morphology of NbC is related to the relative content of Nb and C of the coating. When the contents of Nb and C are low, the primary NbC is relatively small, and the shape of NbC is mainly polygonal having the feature of planar growth. The radius of curvature at the corner of the polygon NbC is small, which makes the concentration of Nb and C higher and has a faster growth rate, thereby rowing into the flower-like shape. When the content of Nb and C increases, due to the anisotropy of the surface tension and the anisotropy of growth dynamics of carbides [28], NbC tends to grow into the cross-dendritic or long strip shape.

Figure 4. SEM images of the surface of the coatings with (**a**) 10.75% Nb-hypereutectic, (**b**) 11.65% Nb-near eutectic (**c**) 12.55%Nb-hypoeutectic.

From Figure 4, it also can be found that the volume fraction of the eutectic regions increases gradually with increasing Nb content. Cr and Nb can reduce the austenite phase region. That is, the eutectic line moves to the lower C content side, resulting in an increase in the volume fraction of the eutectic colonies. Therefore, the simultaneous addition of Cr and Nb leads to increase in the eutectic content of the coatings [18]. Moreover, the presence of MC type carbides have been reported to be more effective in increasing abrasive wear resistance than either raising the eutectic M_7C_3 content or increasing the width of the M_7C_3 eutectic carbide particles [29]. It is believed that the increase in NbC is beneficial to improve the wear resistance of the coatings.

Figure 5 shows the element distribution in the microstructure of Alloy E. Clearly, the maximum Nb concentrations can be seen at the NbC sites. Moreover, the NbC sites are essentially free of Fe and Cr. Kesri and Murand-Charre [30] have reported that the NbC carbide does not contain any substitutional elements, and only a very small amount of Nb can be dissolved into M_7C_3 carbides. Additionally, the maximum Cr concentrations can be seen in the eutectic network around the primary austenite dendrites, owing to low solubility of Cr element in the austenite phase [18]. Fe is mainly concentrated on the primary austenite dendrites.
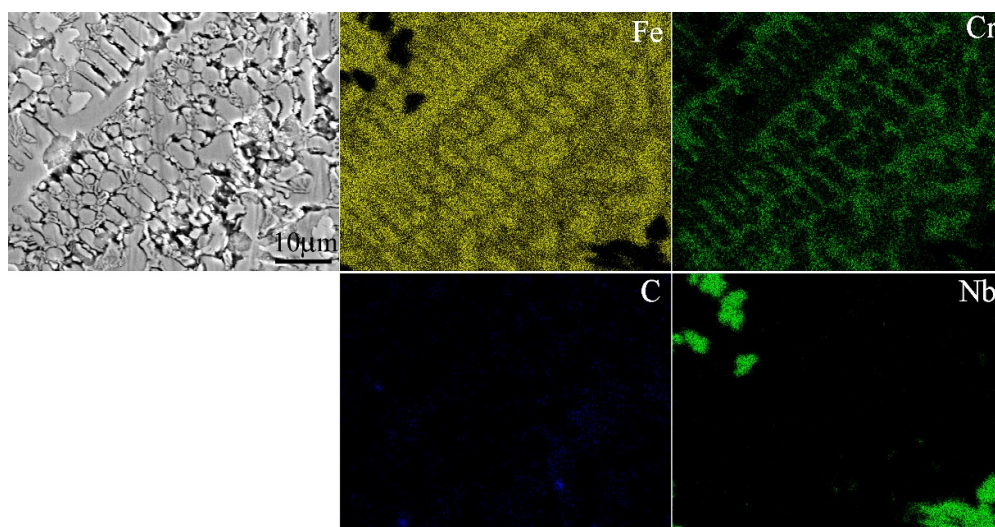

Figure 5. SEM image and EDS element distribution maps of Alloy E coating.

3.3. Hardness and Wear Resistance

Rockwell hardness and mass loss (during wear testing) plotted as a function of the Nb content of the coating are shown in Figure 6. It can be seen that the hardness of the coatings increases firstly and then decreases, while the mass loss decreases firstly and then increases with increasing Nb content. It is well known that the wear resistance is affected by several factors, such as hardness, volume percentage of carbides, and size and distribution of carbides. For Alloy A with only 8.96% Nb content, the coating exhibits a low hardness and a big weight loss due to the small amount of NbC carbides, indicating poor wear resistance. The difference in hardness and mass loss between the coatings of Alloy B and Alloy C is not obvious, but it can still be seen that as the Nb content increases from 8.96% to 10.75%, the hardness increases and the mass loss decreases, corresponding to an improvement in the wear resistance. The coating has the maximum hardness (about 64.6 HRC) and the minimum mass loss when the Nb content is 11.65%. This is due to the transformation of the microstructure from hypereutectic to eutectic. A large quantity of eutectic microstructure forms a strong skeleton structure, resulting in a large number of barriers and limiting the path for dislocation movement, thereby resisting the abrasive wear. However, when the Nb content further increases from 11.65% to 12.55%, the hardness decreases obviously from 64.5 to 56.9 HRC, and the weight loss of Alloy E is nearly four times less than that of Alloy D, corresponding to deterioration of the wear resistance. This may be due to the increase in coarse NbC carbide content leading to increased brittleness of the coating.
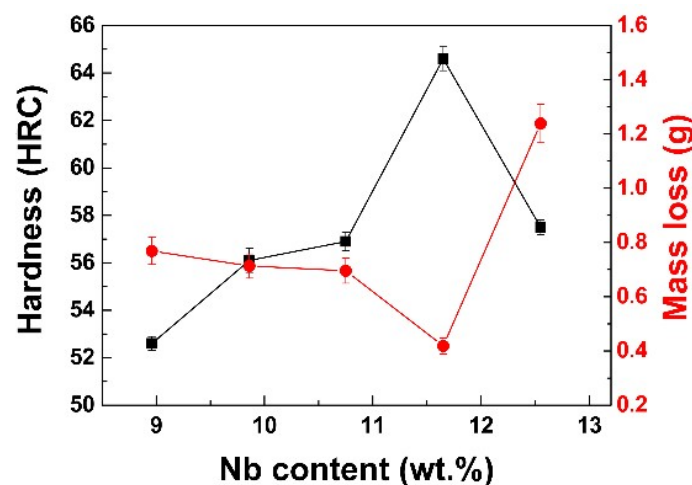

Figure 6. Rockwell hardness and mass loss (during wear testing) plotted as a function of the Nb contents of the coatings.

Figure 7 shows the wear morphologies of Alloy D and Alloy E after wear testing. The wear morphology of Alloy D shows a small quantity of shallow grooves and voids (see Figure 7a,b), indicating that the wear mechanism is dominated by micro-cutting. In general, the hard phase and the soft matrix constituents of wear-resistant materials play different roles: the hard carbides can prevent wear by grooving or indenting mineral particles [31], while the soft matrix with good toughness can effectively protect the carbides [32]. It is considered that the novel microstructure with massive hard and wear-resistant primary NbC carbides distributing uniformly in the fine and strong $\gamma+M_7C_3$ eutectic matrix has excellent wear resistance and good toughness. The NbC carbides with high hardness can blunt the quartz sands and enhance the wear resistance. The wear-resistant primary NbC carbides can also retard the $\gamma+M_7C_3$ eutectic matrix from severe selective wear. A large number of $\gamma+M_7C_3$ eutectic microstructure makes the coating strong, which can effectively resist the abrasive wear, thereby avoiding the deep penetration of abrasive from the coating to the steel substrate. Also, the reduction of the carbon content in coating improves the toughness of coating, which can effectively protect the carbides from cracking during wear. Therefore, it is found that the coating of Alloy D has a much

higher resistance to plastic deformation and scoring, which increases the resistance to plastic erasing or removal of the edges of grooves.
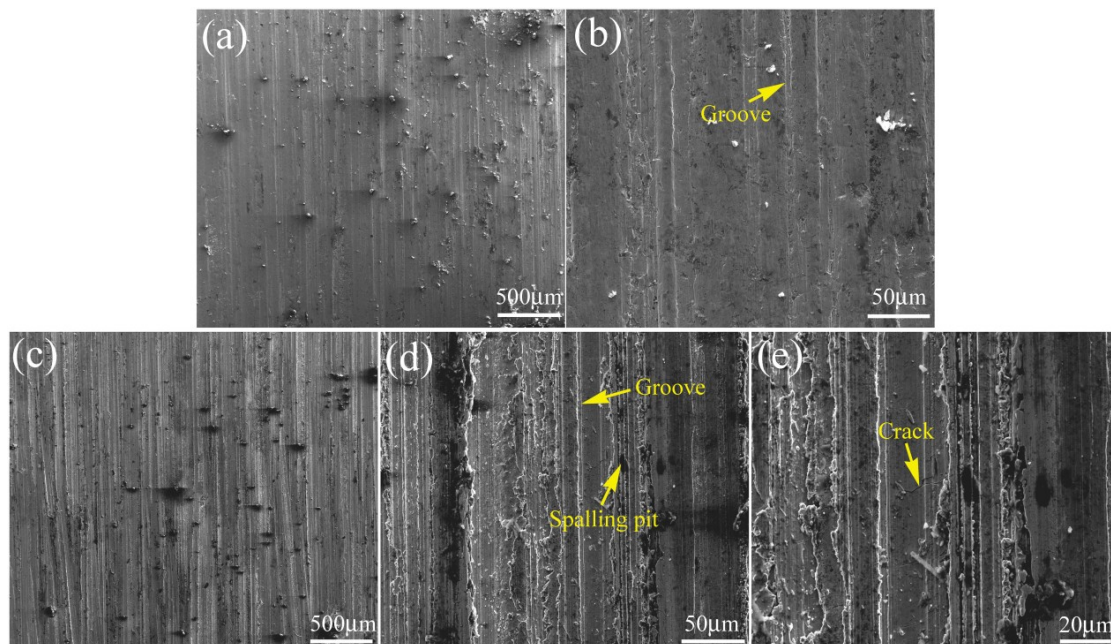

Figure 7. Wear morphology of the various coatings: (**a**,**b**) Alloy D; (**c**–**e**) Alloy E.

The wear morphology of Alloy E is shown in Figure 7c,d. As can be seen, there are numerous deep and long grooves parallel to each other in localized regions, and there are some peeling pits, indicating that the wear mechanism is a combination of abrasion and spallation. Compared with other coatings, although its hardness (about 57.5 HRC) is not the lowest, the wear resistance of Alloy E coating is the worst. The wear morphologies and mechanism are closely related to the microstructures [33]. Therefore, the difference in wear morphology could be attributed to the relatively coarse NbC carbides, resulting in a high brittleness of the coating. It is considered that the coarse NbC carbides can cause stress concentration at the carbide/matrix interface, thereby causing carbide particles to peel off the coating surface. The peeled carbide particles become new abrasive particles, leading to more serious wear on the coating surface, and a lot of deep and long grooves and traces of peeled carbides can be observed on the worn surface [34]. Rafiei et al. have investigated the microstructure and wear behavior of Fe-Ti-V-C cladding alloys and reported similar results [7]. Patrich et al. have reported that the coarse carbide particles are more easily separated by wear particles. The coarser particles have a higher discontinuity at the interface between the particles and matrix in the coatings [35]. The high magnification image (Figure 7e) shows that cracks have formed on the coating surface. Due to the high hardness of the carbide particles, the shearing of these particles is difficult and the microcracks nucleate in the carbides. Some cracks nucleate at the carbide/matrix interface and grow into the carbide body, thus forming large cracks, which causes the carbides to crack and spall off [33]. In addition, due to the low hardness of the γ phase, plastic deformation occurs during the wear process [18]. The existence of the primary γ phase in the hypoeutectic microstructure is the main reason for the plastic deformation to form continuous grooves on the worn surface of Alloy E. In short, the wear resistance of alloyed coating depends not only on the volume fraction and dispersion of the hard phase carbides, but also on the compatibility of the hardness and toughness of the matrix phase of the coating.

4. Conclusions

In this study, Fe-12Cr-*x*Nb-4C coatings with different Nb content were fabricated on commercial low-carbon steel by PTA process. The structure, hardness and wear resistance of the coatings were studied. The main conclusions are as follows:

- The Fe-12Cr-*x*Nb-4C coatings with the Nb contents ranging from 8.96% to 10.75% have a hypereutectic structure composed by martensite, austenite matrix, primary NbC carbides and $\gamma+M_7C_3$ eutecic. As the Nb content increases to 11.65%, it changes to the near-eutectic structure consisting of $\gamma+M_7C_3$ eutectic and NbC carbides. When the Nb content is increased to 12.55%, the coating shows a hypoeutectic structure containing primary γ, $\gamma+M_7C_3$ eutectic and NbC carbides.
- The amount of NbC carbides increases with increasing Nb content. The microstructure of coatings confirms the presence of flower-like, polygonal NbC carbides as the Nb content increases from 8.96% and 10.75% and long strip, cross dendrite NbC carbides in the matrix when the Nb content is 11.65% and 12.55%.
- The hardness and wear resistance of coatings increase firstly and then decrease with increasing Nb content.
- Wear resistance of coating with the 11.65% Nb content is better than that of the other four coatings. The formation of $\gamma+M_7C_3$ eutectic is the most important reason for obtaining good wear resistance.
- The coating with 12.55% Nb content has the worst wear resistance, owing to high brittleness of the coarse NbC carbides accelerating abrasion damage of the coating.

References

1. Hawk, J.A.; Wilson, R.D.; Danks, D.R.; Kiser, M.T. Abrasive wear failures. In *Failure Analysis and Prevention*; Becker, W.T., Shipley, R.J., Eds.; ASM Handbook: Cleveland, OH, USA, 2002; Volume 11, pp. 906–921.
2. Li, G.; Gan, Y.J.; Liu, C.H.; Shi, Y.; Zhao, Y.C.; Kou, S.Z. Corrosion and wear resistance of Fe-based amorphous coatings. *Coatings* **2020**, *10*, 73. [CrossRef]
3. Kwak, S.Y.; Yun, J.G.; Lee, J.H.; Shin, D.I.; Kang, C.Y. Identification of intermetallic compounds and its formation mechanism in boron steel hot-dipped in Al-7 wt.% Mn alloy. *Coatings* **2017**, *7*, 222. [CrossRef]
4. Yury, K.; Filippov, M.; Makarow, A.; Malygina, I.; Soboleva, N.; Fantozzi, D.; Andrea, M.; Koivuluoto, H.; Vuoristo, P. Arc-sprayed Fe-based coatings from cored wires for wear and corrosion protection in power engineering. *Coatings* **2018**, *8*, 71. [CrossRef]
5. Hu, J.; Jiang, J.; Li, H.; Yang, X.; Xu, H.; Jin, Y.; Ma, C.; Dong, Q.; Guo, N. Effect of annealing treatment on microstructure and properties of Cr-coatings deposited on AISI 5140 steel by brush-plating. *Coatings* **2018**, *8*, 193. [CrossRef]
6. Pogrebnjak, A.D.; Beresnev, V.M.; Bondar, O.V.; Postolnyi, B.O.; Zaleski, K.; Coy, E.; Jurga, S.; Lisovenko, M.O.; Konarski, P.; Rebouta, L.; et al. Superhard CrN/MoN coatings with multilayer architecture. *Mater. Des.* **2018**, *153*, 47–59. [CrossRef]
7. Rafiei, M.; Ghayour, H.; Mostaan, H.; Hosseini, M.Z. The effect of V addition on microstructure and tribological properties of Fe-Ti-C claddings produced by gas tungsten arc welding. *J. Mater. Process. Technol.* **2019**, *266*, 569–578. [CrossRef]

8.　Liu, D.S.; Wang, J.Y.; Zhang, Y.; Kannan, R.; Long, W.; Wu, M.F.; Wang, Y.Y.; Li, L.J. Effect of Mo on microstructure and wear resistance of slag-free self-shielded metal-cored welding overlay. *J. Mater. Process. Technol.* **2019**, *270*, 82–91. [CrossRef]

9.　Hao, W.; Sheng, F.Y.; Adnan, R.K.; An, G.H. Effects of vanadium on microstructure and wear resistance of high chromium cast iron hardfacing layer by electroslag surfacing. *Metals* **2018**, *8*, 458.

10.　Gou, J.F.; Wang, Y.; Sun, J.P.; Li, X.W. Bending strength and wear behavior of Fe-Cr-C-B hardfacing alloys with and without rare earth oxide nanoparticles. *Surf. Coat. Technol.* **2017**, *311*, 113–126. [CrossRef]

11.　Maksakova, O.V.; Simoẽs, S.; Pogrebnjak, A.D.; Bondar, O.V.; Kravchenko, Y.O.; Koltunowicz, T.N.; Shaimardanov, Z.K. Multilayered ZrN/CrN coatings with enhanced thermal and mechanical properties. *J. Alloy. Compd.* **2019**, *776*, 679–690. [CrossRef]

12.　Brezinová, J.; Draganovská, D.; Guzanová, A.; Balog, P.; Viááš, J. Influence of the hardfacing welds structure on their wear resistance. *Metals* **2016**, *6*, 36. [CrossRef]

13.　Moghaddam, H.Z.; Sharifitabar, M.; Roudini, G. Physical and mechanical properties of nanostructured (Ti-Zr-Nb)N coatings obtained by vacuum-arc deposition method. *Surf. Coat. Technol.* **2019**, *361*, 91–101.

14.　Zong, L.; Guo, N.; Li, R.G.; Yu, H.B. Effect of B content on microstructure and wear resistance of Fe-3Ti-4C hardfacing alloys produced by plasma-transferred arc welding. *Coatings* **2019**, *9*, 265. [CrossRef]

15.　Carrington, M.J.; Daure, J.; Ratia, V.L.; Shipway, P.H.; McCartey, D.G.; Stewart, D.A. Microstructural characterisation of Tristelle 5183 (Fe-21%Cr-10%Ni-7.5%Nb-5%Si-2%C in wt%) alloy powder produced by gas atomisation. *Mater. Des.* **2019**, *164*, 107548. [CrossRef]

16.　Li, Q.T.; Lei, Y.P.; Fu, H.G. Growth mechanism, distribution characteristics and reinforcing behavior of (Ti, Nb)C particle in laser cladded Fe-based composite. *Appl. Surf. Sci.* **2014**, *316*, 610–616. [CrossRef]

17.　Zhao, C.C.; Xing, X.L.; Guo, J.; Shi, Z.J.; Zhou, Y.F.; Ren, X.J.; Yang, Q.X. Micro-properties of (Nb,M)C carbide (M=V, Mo, V, W and Cr) and precipitation behavior of (Nb,V)C in carbide reinforced coating. *J. Alloys Compd.* **2019**, *788*, 852–860. [CrossRef]

18.　Sadeghi, F.; Najafi, H.; Abbasi, A. The effect of Ta substitution for Nb on the microstructure and wear resistance of an Fe-Cr-C hardfacing alloy. *Surf. Coat. Technol.* **2017**, *324*, 85–91. [CrossRef]

19.　Yang, K.; Gao, Y.; Yang, K.; Bao, Y.F.; Jiang, Y.F. Microstructure and wear resistance of Fe-Cr13-C-Nb hardfacing alloy with Ti addition. *Wear* **2017**, *376–377*, 1091–1096. [CrossRef]

20.　Zhang, L.M.; Sun, D.B.; Yu, H.Y. Effect of niobium on the microstructure and wear resistance of iron-based alloy coating produced by plasma cladding. *Mater. Sci. Eng. A* **2008**, *490*, 57–61. [CrossRef]

21.　Correa, E.O.; Alcantara, N.G.; Valeriano, L.C.; Barbedo, N.D.; Chaves, R.R. The effect of microstructure on abrasive wear of a Fe-Cr-C-Nb hardfacing alloy deposited by the open arc welding process. *Surf. Coat. Technol.* **2015**, *276*, 479–484. [CrossRef]

22.　Chung, R.J.; Tang, X.; Li, D.Y.; Hinckley, B.; Dolman, K. Microstructure refinement of hypereutectic high Cr cast irons using hard carbide-forming elements for improved wear resistance. *Wear* **2013**, *301*, 695–706. [CrossRef]

23.　Yang, J.; Huang, J.H.; Fan, D.Y.; Chen, S. Microstructure and wear properties of Fe-6wt.%Cr-0.55wt.%C-Xwt.%Nb laser cladding coating and the mechanism analysis. *Mater. Des.* **2015**, *88*, 1031–1041. [CrossRef]

24.　*ASTM A283/A283M-18 Standard Specification for Low and Intermediate Tensile Strength Carbon Steel Plates*; ASTM: West Conshohocken, PA, USA, 2018.

25.　Zhang, Z.Q.; Shen, P.; Wang, Y.; Dong, Y.P.; Jiang, Q.C. Fabrication of TiC and TiB$_2$ locally reinforced steel matrix composites using a Fe-Ti-B$_4$C-C system by an SHS-casting route. *J. Mater. Sci.* **2007**, *42*, 8350–8356. [CrossRef]

26.　Radzikowska, J.M. Metallography and microstructures of cast iron. In *Metallography and Microstructures*; Vander Voort, G.F., Ed.; ASM Handbook: Cleveland, OH, USA, 2004; Volume 9, pp. 565–587.

27.　Filipovic, M.; Kamberovic, Z.; Korac, M.; Gavrilovski, M. Microstructure and mechanical properties of Fe-Cr-C-Nb white cast irons. *Mater. Des.* **2013**, *47*, 41–48. [CrossRef]

28.　Wang, Z.H.; Wang, H.; He, D.Y.; Cui, L.; Jiang, J.M.; Zhou, Z.; Zhao, Q.Y. Microstructure characterization of in situ NbC/high entropy alloys by plasma cladding. *Rare Met. Mater. Eng.* **2015**, *44*, 3156–3160.

29.　Qiu, W.B.; Liu, Y.; Yea, J.W.; Fan, H.J.; Qiu, Y.C. Effects of (Ti,Ta,Nb,W)(C,N) on the microstructure, mechanical properties and corrosion behaviors of WC-Co cemented carbides. *Ceram. Int.* **2017**, *43*, 2918–2926. [CrossRef]

30. Kesri, R.; Durand-Charre, M. Phase equilibria, Solidification and solid-state transformations of white cast irons containing niobium. *J. Mater. Sci.* **1987**, *22*, 2959–2964. [CrossRef]

31. Azimi, G.; Shamanian, M. Effect of silicon content on the microstructure and properties of Fe-Cr-C hardfacing alloys. *J. Mater. Sci.* **2012**, *45*, 842–849. [CrossRef]

32. Bourithis, L.; Papadimitriou, G.D. The effect of microstructure and wear conditions on the wear resistance of steel metal matrix composites fabricated with PTA alloying technique. *Wear* **2009**, *266*, 1155–1164. [CrossRef]

33. Zum Gahr, K.-H. *Microstructure and Wear Mechanism*, 1st ed.; Elsevier: North Holland, The Netherlands, 1987.

34. Correa, E.O.; Alcantara, N.G.; Tecco, D.G.; Kuma, R.V. The relationship between the microstructure and abrasive resistance of a hardfacing alloy in the Fe-Cr-C-Nb-V system. *Mater. Sci. Eng. A* **2007**, *38*, 1671–1680. [CrossRef]

35. Patrich, L.; Li, W.; Xing, S.; Nazmul, A. Comparison of abrasive wear of a complex high alloy hardfacing deposit and WC-Ni based metal matrix composite. *Wear* **2002**, *294*, 380–386.